Ukrainian Journal of Physical Optics
ISSUE 2
2024

TRIBOLOGICAL PROPERTIES OF TEXTURED TITANIUM-ALLOY SURFACE UNDER DRY-SLIDING AND WATER-LUBRICATION CONDITIONS

GUOJUN DENG [1] AND JIALIANG GUO [1, 2]

[1] Research Department for New-Display Technologies, Jihua Laboratory, Foshan 528251, China
[2] School of Electrical and Information Engineering, Zhengzhou University, Zhengzhou 450001, China gsafeg@163.com

Received: 20.11.2023

Abstract. A flexible and efficient solution is developed to enhance the performance and extend the service life of a Ti6–Al4–V titanium alloy. This solution combines a commercially available nanosecond laser-based metal-surface patterning technique with a self-assembled molecular-film modification. The surface of the titanium alloy is patterned with periodic dimple arrays of varying densities and depths using the laser processing. The surface morphology, roughness and chemical composition of our samples are analyzed using a scanning electron microscopy and a confocal microscopy. Moreover, the wettability of the modified titanium-alloy surface is assessed with a contact-angle meter, yielding in a maximum contact angle as large as 153.2°. The coefficient of friction is measured using a tribometer and the wear mechanism is analyzed with a study of surface morphology. Under dry-sliding and water-lubrication conditions, the average coefficient of friction is reduced respectively by over 20% and 60%, when compared to the value typical for the original surface. This reduction is attributed to changed surface roughness and wettability. Our method offers a practical and efficient means of enhancing the wettability and the tribological performance of the titanium-alloy surfaces.

Keywords: coefficient of friction, laser texturing, titanium alloys, wear scars, wettability
UDC: 621.7+535
DOI: 10.3116/16091833/Ukr.J.Phys.Opt.2024.02043

1. Introduction

Titanium, the fourth most abundant metal in the Earth's crust, is regarded as a highly promising "green material" [1]. Due to its high heat-dissipation efficiency, high resistivity, exceptional specific fracture toughness, good fatigue strength and crack-extension resistance [2], titanium alloys have been widely adopted as structural materials for micro-components in various industries such as railway construction, aviation, biomedicine, and petrochemical industry [3]. However, titanium alloys suffer from poor wear resistance and a high coefficient of friction (CoF). The ratio of surface area to volume increases with decreasing component size, resulting in increased surface effects, wear and surface adhesion. These issues affect considerably reliability and stability of titanium-based components and hamper many potential applications [4]. Practical examples of this problem include a failure of oil field-anchor cables due to fretting wear [5] and a generation of wear particles in Ti-based artificial hip joints, which causes bone resorption and aseptic loosening [6]. Therefore, a surface treatment is a necessary step to enhance tribological properties of titanium alloys.

Traditional surface-treatment methods include ion implantation [7], thermal spraying [8] and carburization [9, 10]. Morozow et al. [11] have applied the ion implantation to create an extra-hard W_2N coating on the surface of WC–Co alloy-based guide pads, which has led to a more than 2.5-fold increase in the durability of deep-hole drills. Bhosale et al. [12] have

conducted a systematic investigation of the tribological properties of WC–Cr_3C_2–Ni coating produced through high-speed oxyfuel spraying. They have demonstrated an excellent wear resistance above 500°C, which can be attributed to homogeneous formation of WO_3. Sahu et al. [13] have used a surface mechanochemical carburization treatment to create a hard Fe_3C phase and a nanocrystalline surface layer on Ni-Cr-Mo steel, which reduces the surface-wear rate to one-fifth of its original value. However, all of these methods aim to enhance the wear resistance by increasing the surface hardness of the alloys, with little focus on reducing friction. The lubricity and wear resistance of a surface are closely related to its morphology [14, 15]. As a result, laser-texturing technologies for creating rough regularly arranged structures on the alloy surfaces, with inducing no phase changes, have become a popular research area for improving tribological properties. Some earlier studies [16–19] have been conducted under dry-sliding conditions with no consideration of a lubricating medium. Some other studies have used polymer-based lubricants [20] or artificial body fluids [21] as lubricants to simulate some tribological behaviour under different scenarios. Water as a lubricating medium offers some advantages in terms of safety, energy efficiency and environmental friendliness, especially for superhydrophobic surfaces.

In this study, we utilize laser processing to create dimple-array microstructures with different surface densities and depths on the surface of a Ti6–Al4–V alloy. After that, a textured surface is coated with a molecular layer of 1H,1H,2H,2H-perfluorooctyl trichlorosilane [$CF_3(CF_2)_5(CH_2)_2SiCl_3$] (FOTS) by using a molecular-film self-assembly method. This results in the preparation of titanium-alloy surfaces with different surface morphologies and wettabilities. The tribological properties of these samples have been evaluated under both dry-sliding and water-lubrication conditions, using a mechanical tester and a tribometer. This approach can testify a relevance of the impact of surface morphology and wettability on the tribological behaviour of titanium alloys, thus providing both technical means and theoretical support for the fabrication of wear-resistant titanium-alloy surfaces.

The remainder of this article is structured as follows. Section 2 describes our experimental materials and methods. Section 3 presents and discusses the results of our experiments. Finally, Section 4 draws the main conclusions.

2. Materials and Methods

A substrate material used in this study was a Ti6–Al4–V titanium-alloy disk with the thickness 7 mm and the diameter 25 mm. Before laser processing, a substrate underwent a preparation process that included sequentially grounding with 400, 600 and 800 mesh diamond sandpaper and then polishing with a polishing machine until the surface roughness (Sa) was less than 0.2 μm. A sample was rinsed in an ultrasonic bath in petroleum ether, absolute ethanol and distilled water in sequence for 5 min prior to laser processing, in order to remove any impurities and oil stains.

As shown in Fig. 1, laser processing was performed using a pulsed fibre laser (Sundor P50QB, China) with the output power 50 W, the central wavelength 1064 nm, the pulse width 130 ns, the repetition frequency 40 kHz and the beam quality $M^2 < 1.8$. A laser beam was converged using an F-Theta lens with the 254-mm focal length, thus creating, point by point, a dimple array composed of circular pits with the approximate diameters 100 μm on the material surface under atmospheric conditions. A computer-controlled light-wave scanner based on a two-axis galvanometer was used with the laser, which allowed for

creating a set of micro-dimple textures with different densities and depths, while adjusting the dimple interval and the laser-scanning cycle. After laser ablation, the samples were continuously irradiated by a 250 W ultraviolet lamp for 1 h and then immersed in a 3 wt% FOTS isooctane solution for 2 h. FOTS bonds with hydroxyl groups on the surface of the titanium alloy reduced considerably the surface energy. Finally, the samples were ultrasonically cleaned in petroleum ether, anhydrous ethanol and distilled water in sequence for 5 min and then blown dry with nitrogen to complete the preparation process.

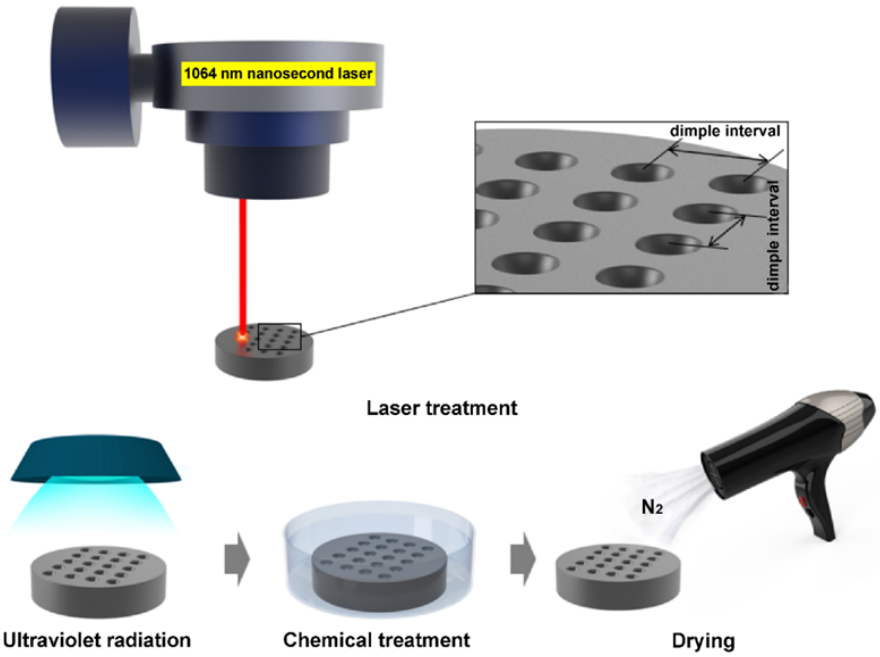

Fig. 1. Scheme of a process of preparation of a superhydrophobic Ti6–Al4–V titanium alloy surface.

The three-dimensional surface morphology and the roughness (Sa; an arithmetic mean height) of the samples were observed and analyzed using a confocal microscope (Olympus LEXTTM OLS5100, Japan). The two-dimensional surface morphology and the chemical composition were determined using either a scanning electron microscopy or an energy-dispersive X-ray spectroscopy (SEM/EDX, Zeiss Supra 25, Germany). The surface wettability was evaluated by measuring the static water-contact angle (WCA) of a 3-μL droplet of distilled water placed on the sample surface. The WCA was captured using a contact-angle meter (DataPhysics OCA25, Germany) and calculated using a known Laplace–Young equation [22]. The average WCA was calculated from five different locations on each sample. A tribometer (Bruker UMT-5, USA) was used to analyze the variation in the CoF of the samples before and after laser processing. The experiment was conducted under dry-sliding and water-sliding conditions. A linear reciprocating friction test was performed using a ball-on-disk friction tester with a 10 mm Si_3N_4 ceramic ball as a counterpart. During the experiment, the titanium-alloy sample was stationary, while the counterpart was reciprocated at the load of 1 N, with the stroke 6 mm, the frequency 1 Hz and the friction time 600 s. Real-time CoF data were recorded automatically by a computer during our test and the average CoF was calculated. Each group of our experiments was repeated three times to ensure their statistical significance.

3. Results and Discussion

The average depth of the individual dimples appearing after 1, 3 and 5 laser scans are approximately equal to 2.5, 7.0 and 10.0 μm, respectively. Let us consider the samples at the dimple interval 150 μm after 3 laser scans (see Fig. 2a, b). Then the area with concentrated laser energy reaches the ablation threshold of the titanium alloy, which causes the material to burn and remove and so leads to regularly spaced dimple arrays. Bulge structures with the height 5 μm are formed around the dimples, while a few small splashed particles are observed on the surface area where no laser processing is available. When the dimple interval decreases to 80 μm (see Fig. 2c, d), one can observe micro-hills which are formed by mutual stacking and solidification of melted materials. This results in further elevation of the bulges on the sample surface.

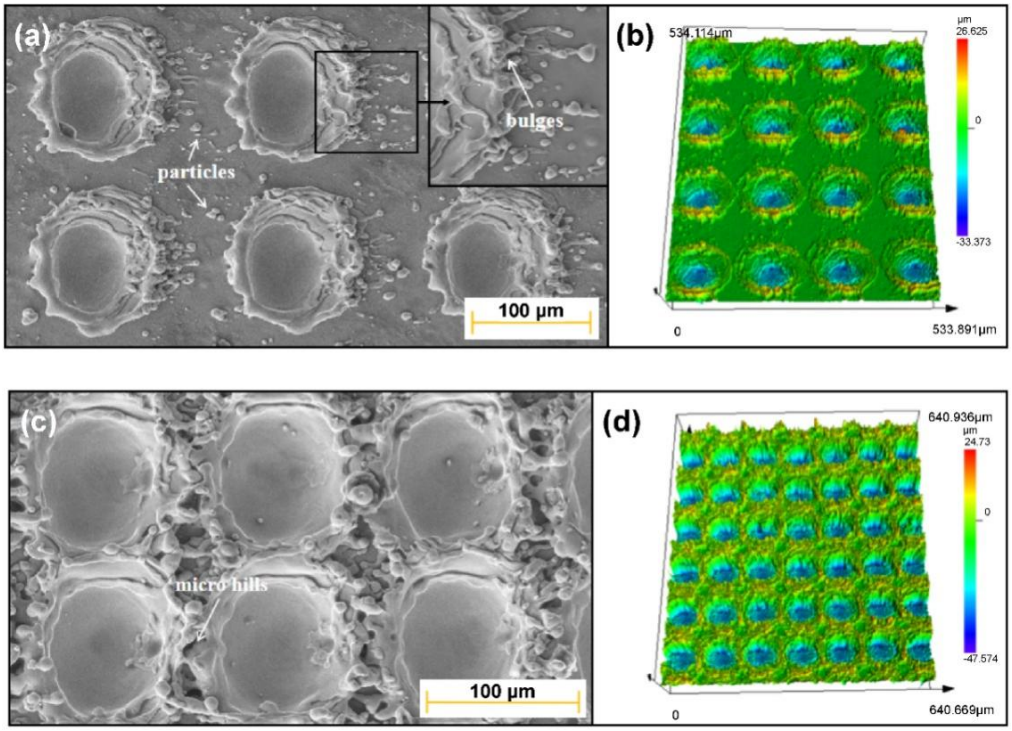

Fig. 2. Textured surface topographies observed after 3 laser scans with the dimple intervals 100 μm (panels (a) and (b)) and 150 μm (panels (c) and (d)): panels (a) and (c) show the SEM images, and panels (b) and (d) the three-dimensional profiles.

The dependences of the surface roughness on the dimple interval are shown in Fig. 3. When only the number of laser-scanning cycles changes, the Sa parameter increases with increasing number of laser-scanning cycles. When the dimple interval is fixed at 80 μm and the number of laser-scanning cycles changes, Sa of the textured surfaces reaches its maximum and then decreases with increasing number of the scanning cycles. When the dimple interval is equal to 50 μm, which is smaller than the dimple diameter, parts of the micro-hills become removed due to overlapping dimples, thus resulting in Sa decrease.

The WCA and the chemical composition of the polished surfaces are illustrated in Fig. 4. The WCA of the polished surface exhibits the hydrophobicity equal to 108.6 ± 0.7° after treatment with FOTS, which can be compared to the value 67.1 ± 3.2° corresponding to the original titanium alloy. This suggests that long chain molecules of FOTS are successfully bound

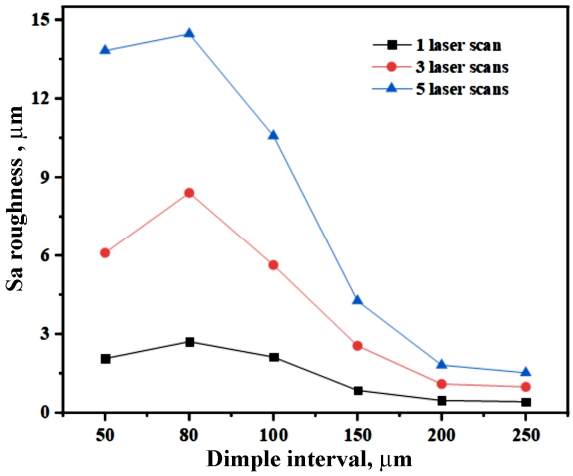

Fig. 3. Dependences of sample-surface roughness on dimple interval, as observed after different numbers of laser-scanning cycles (see the legend).

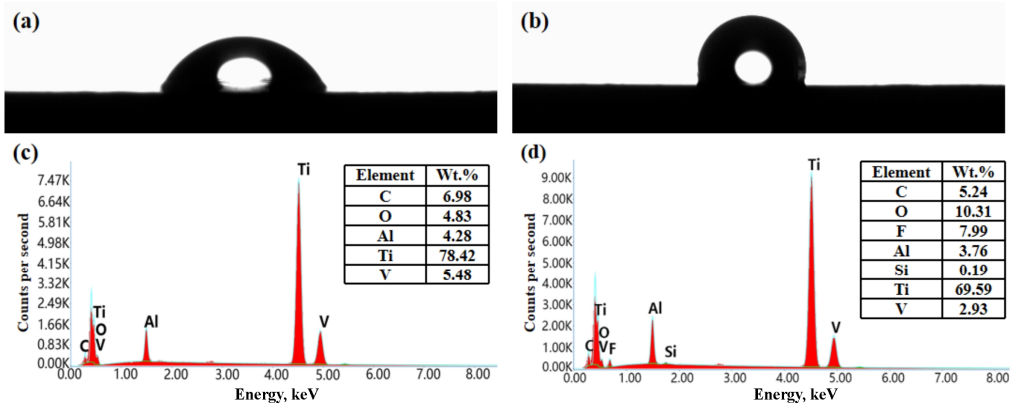

Fig. 4. WCAs (panels (a) and (b)) and chemical compositions (panels (c) and (d)) of polished surfaces: panels (a) and (c) correspond to the original surface, and panels (b), (d) to the chemically modified surface after its treatment with FOTS.

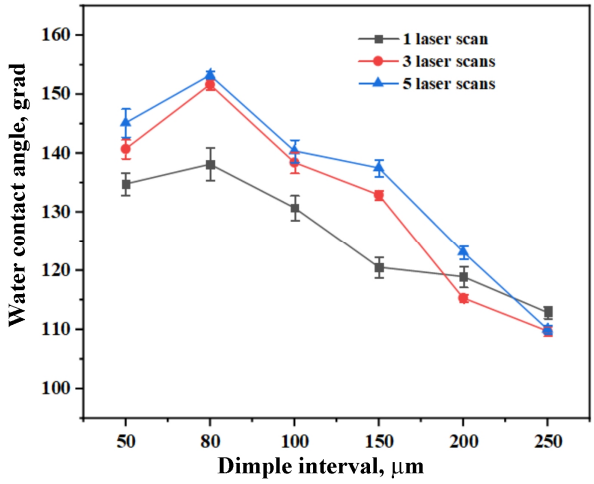

Fig. 5. Dependences of WCAs on dimple interval for the samples prepared at different numbers of laser-scanning cycles (see the legend).

to the substrate surface and they alter its surface wettability. This has been verified by the availability of F and Si in the energy spectrum of the chemically modified surface. The results of the WCA measurements are shown in Fig. 5. Similar to the trend observed for Sa with

changing dimple intervals, the maximum WCA is reached for all the three laser-processing conditions whenever the dimple interval is equal to 80 μm. This indicates that the wettability of the titanium surface patterned with the dimple array correlates with Sa, i.e. the WCA increases with increasing Sa. When Sa < 2μm, the WCAs of the surfaces obtained with different numbers of laser-scanning cycles decreases to a level similar to that of the polished surfaces.

According to the Cassie–Baxter model [23], a droplet is in contact with a solid surface itself, simultaneously interacting with air pockets in the micro-structures of these droplet and solid surface. At this point, the WCA satisfies the following equation:

$$\cos\theta = f_1\cos\theta_1 + f_2\cos\theta_2\,, \tag{1}$$

where θ is the measured WCA, θ_1 and θ_2 denote the intrinsic WCAs respectively of the air and the solid surface, and f_1 and f_2 are the fractions of air and solid in the entire contact area. Note that the conditions $\theta_1 = 180°$ and $f_1 + f_2 = 1$ hold true. Therefore, the measured θ value decreases with increasing solid–liquid area fraction f_2 and increases with increasing air–liquid area fraction f_1. When the laser-scanning cycles are performed sparingly or when the dimples are sparsely distributed, the dimple is shallow or the height of the micro-hills (i.e., bulges on the textured surface) is small. This enables the droplets to enter easily the dimples, which results in a larger fraction of the solid–liquid contact area and so a further decrease in the WCA. With increasing number of the laser-scanning cycles or decreasing dimple interval, the height difference for a concave-convex structure on the textured surface increases. Under this condition, a combination of the micron-scale texture and a nanoscale FOTS-molecular film layer facilitates formation of more air pockets, which hinders the entrance of droplets into the dimples and increases the fraction of the air–liquid contact area. Moreover, when the dimple interval is equal to 80 μm, a super-hydrophobicity property is attained for the surface of the titanium-alloy samples, which is characterized by the WCAs 151.6 ± 0.9° and 153.2 ± 0.6° obtained after 3 and 5 laser-scanning cycles, respectively.

Fig. 6a compares the average CoF values obtained for the non-textured substrate and the textured samples during dry sliding. The data suggests that variations in the dimple interval and the depth within a certain range have a limited impact on the average CoF of the

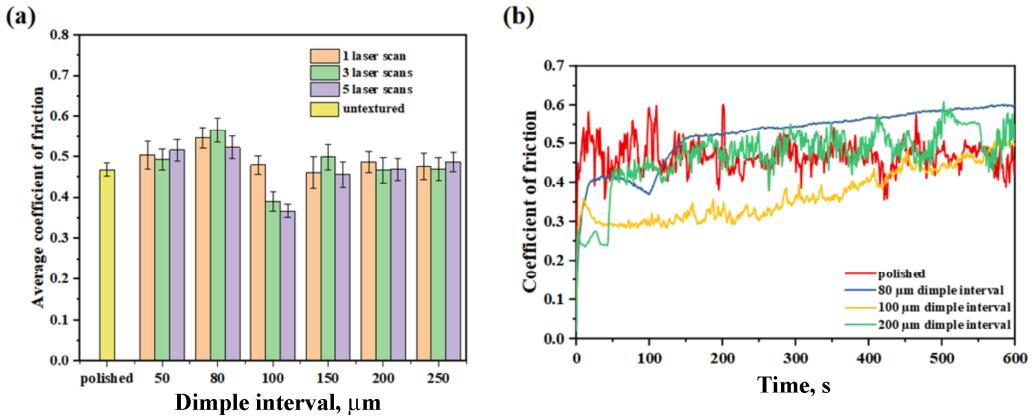

Fig. 6. CoF values obtained under dry-sliding conditions: panel (a) shows the average CoFs of polished surface and samples obtained after different numbers of laser-scanning cycles, and panel (b) corresponds to the real-time CoFs of polished surface and representative samples obtained after 5 cycles of laser scanning.

textured titanium-alloy surfaces, so that most of the values are close to that typical for the polished surface (0.47). In particular, the textured samples with the dimple interval 100 μm reveal the average CoFs 0.39 and 0.37 respectively after 3 and 5 laser-scanning cycles, i.e. they demonstrate a moderate reduction of 17% and 21% if compared to that typical for the original surface. This slight improvement can be attributed to a capturing effect of the dimples on wear debris [24]. When the dimple interval amounts to 80 μm, the micro-hills appearing during sliding in the contact area between the sample surface and the Si_3N_4 ball yield in a somewhat higher average CoF, if compared to the value obtained for the original surface. The real-time CoFs of several representative samples obtained with 5 laser-scanning cycles are shown in Fig. 6b. The polished surface shows an abrupt increase in the CoF above 0.4 at the onset of friction, which is followed by the fluctuations between the values 0.35 and 0.6. The initial CoF of the dimple array with the interval 80 μm is approximately equal to 0.4. However, the roughness of the surface leads to increasing frictional drag [25], causing a gradual continuous increase in the CoF up to 0.6. In contrast, the dimple interval 100 μm corresponds to a smaller CoF (if compared to the value typical for original surface) throughout the overall test, because of a superior ability to accommodate wear debris. Finally, the dimple interval 200 μm corresponds to a similar trend at the onset of friction. However, the dimples are gradually filled with wear debris as the friction continues, which leads to the CoF trend similar to that observed for the polished surface [26].

Fig. 7a shows the average CoFs obtained for different samples under the water-lubrication conditions. The average CoF of most surfaces remains lower than that of the polished surface, which is characterized by the value 0.45. In the case of 5 laser-scanning cycles, the dimple-textured surfaces with the 80-μm and 100-μm intervals reveal respectively the average CoFs 0.2 and 0.17, i.e. they decrease by 56% and 62%, if compared to the value typical for the polished surface. This suggests that the textured surface with FOTS self-assembled molecular film plays a significant role in reducing friction in the water environment [27]. However, in the case of a single laser-scanning cycle, this effect is not as noticeable. With increasing number of laser-scanning cycles, deeper dimples appear which can promote hydrodynamic lubrication, enhance the bearing capacity of the surface, reduce the friction and so achieve a lower CoF [28]. Fig. 7b shows the real-time CoFs obtained for different samples under the water-

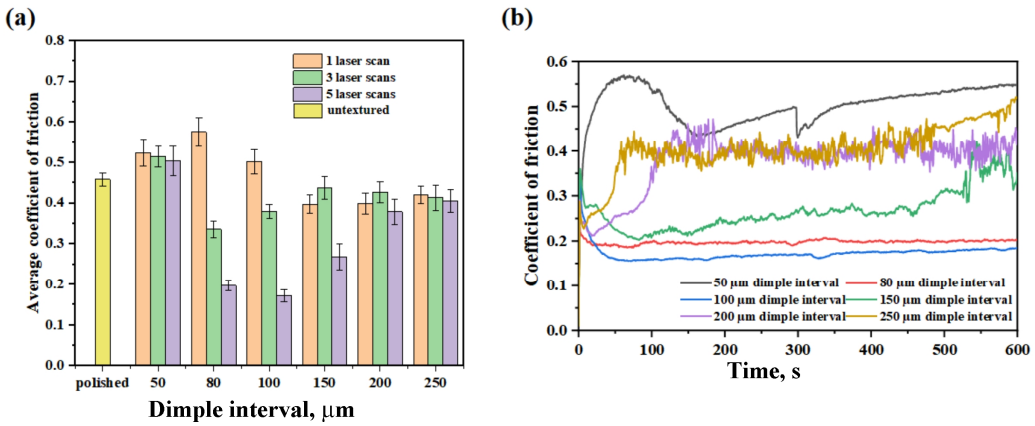

Fig. 7. CoFs values obtained under water-lubrication conditions: panel (a) shows the average CoFs of polished surface and samples obtained after different numbers of laser-scanning cycles, and panel (b) corresponds to the real-time CoFs of samples obtained after 5 cycles of laser scanning.

lubrication conditions after 5 laser-scanning cycles. The real-time CoF for the surface with the 50-μm dimple interval is mainly affected by enhanced frictional drag arising because of a dense surface texture. This gives the CoF values larger than those obtained for the other textured surfaces during the whole test period. For the 80-μm and 100-μm dimple intervals, the textured surfaces form a hydrophobic boundary lubricating film with excellent anti-friction properties [29, 30], which causes the CoF to remain stable below 0.2 after the initial decrease. For the 150-μm dimple interval, the CoF shows a mild increase but still remains below 0.3 at the early stages of friction. However, the CoF increases rapidly above 0.4 when the friction lasts over 500 s, since the boundary lubricating film on the non-superhydrophobic texture is fragile. The friction between the Si_3N_4 ball and the sample surface generates heat, which increases gradually the temperature of the self-assembled molecular film [31]. Therefore the boundary lubricating film eventually disappears and causes a failure. For the dimple-textured surfaces with the intervals 200 and 250 μm, capturing and reducing wear debris appearing through the texture become the major factor that affects the CoF, which is limited by the hydrophobicity with the WCA < 130°. Under these conditions, the dimple array with the interval 250 μm is filled with the wear debris after 60 s of sliding, so that the two samples show a similar real-time CoF trend after approximately 100 s. In comparison with the case of dry sliding, a longer time is needed to increase the CoF from below 0.3 to 0.4 in the water-lubrication scenario. This is because a modification of low surface energy reduces the free energy at the sample surface and hinders the adsorption of the sample surface onto the Si_3N_4 ball. In addition, water can have a scouring effect on the wear debris.

Fig. 8 shows the wear scars observed for different samples. Under the dry-sliding conditions, deep dark gray wear scars appear on the polished surface (see Fig. 8a), with an obvious plowing effect. Then the dominant form of wear is adhesive. For the dimple-textured surface with the interval 80 μm, the wear scar from the dry friction (see Fig. 8b) is shallow, with a switch to the abrasive wear, since the dimples capture small abrasive particles and reduce the plowing effect. The same surface reveals a shallower and narrower wear scar under the water-lubrication conditions (see Fig. 8c), when compared to the dry-sliding conditions. The equation suggested by Jung and Bushan [32] can be used to explain the force between the Si_3N_4 ball and the surface of the titanium-alloy samples:

$$F = 2\pi R\gamma\left(\cos\theta_3 + \cos\theta_4\right), \tag{2}$$

where F, θ_3, θ_4, R and γ represent respectively the force generated between the Si_3N_4 ball and

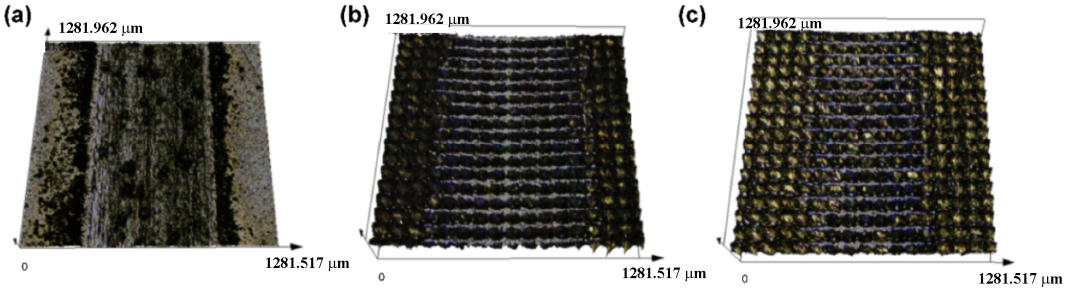

Fig. 8. Wear scars observed on the surfaces of our samples: (a) polished surface under dry-sliding conditions, (b) textured surface with the dimple interval 80 μm obtained after 5 cycles of laser scanning under dry-sliding conditions, and (c) textured surface with the dimple interval 80 μm obtained after 5 cycles of laser scanning under water-lubrication conditions.

the surface of the titanium-alloy sample, the WCA of the sample surface, the WCA of the Si_3N_4 ball, the radius of the Si_3N_4 ball and surface tension of the lubricating medium. For the surfaces of hydrophobic samples with the WCA > 90°, $\cos\theta_1$ is negative. This can reduce significantly the *F* term and so decrease the adhesion and the friction of the surface.

4. Conclusions

A nanosecond-pulse laser has been utilized to fabricate periodic dimple-based arrays on the surface of the titanium alloy. Our aim is improving the surface performance through a combination of laser texturing and chemical modification performed using a self-assembled molecular layer. The impact of number of the laser scans and the dimple intervals on the sample morphology, roughness and wettability has been thoroughly evaluated. The results testify that a combination of the chemical modification and the laser texturing increases the WCA of the titanium-alloy surface from the initial value 67° to more than 153°. The tribological behaviour of the sample surfaces has also been analyzed through the CoF measurements. The average CoF is reduced by up to 21% and 61% respectively under the dry-sliding and water-lubrication conditions, thus indicating a high efficiency of the superhydrophobic surface with compact deep dimples in reinforcing lubrication, particularly during water sliding.

Furthermore, the wear mechanisms of the surfaces have been studied. Our results indicate a shift from adhesive wear to abrasive wear arising due to the surface texturing. When compared to the previous study [15], we have achieved an improved anti-wear effect under the water-lubrication conditions, using a lower-cost laser and a more time-efficient laser-scanning approach. This enhancement can be attributed to the superhydrophobic properties of the surface. Simultaneously, we observe that, although the micro-grooves ablated by the picosecond lasers manifest a better regularity, the random structures (such as micro-hills and splatters) induced by the nanosecond lasers tend to result in a larger WCA for the surface. A potential for applications of our methods to large assemblies such as aircraft or vessel skins should be further explored in the future.

Funding. This work is supported by the Jihua Laboratory Foundation of Guangdong Province Laboratory, China (the Grant X220341TE22J).

Disclosures. The authors declare no conflict of interest.

References

1. Nagase, T., Hori, T., Todai, M., Sun, S. H., & Nakano, T. (2019). Additive manufacturing of dense components in beta-titanium alloys with crystallographic texture from a mixture of pure metallic element powders. *Materials & Design*, *173*, 107771.
2. Gao, F., Guo, Y., Qiu, S., Yu, Y., & Yu, W. (2020). Fracture toughness of friction stir welded TA5 titanium alloy joint. *Materials Science and Engineering: A*, *776*, 138962.
3. Cui, C., Hu, B., Zhao, L., & Liu, S. (2011). Titanium alloy production technology, market prospects and industry development. *Materials & Design*, *32*(3), 1684-1691.
4. Pohrelyuk, I. M., Sheykin, S. E., Padgurskas, J., & Lavrys, S. M. (2018). Wear resistance of two-phase titanium alloy after deformation-diffusion treatment. *Tribology International*, *127*, 404-411.
5. Xie, R., Lin, N., Zhou, P., Zou, J., Han, P., Wang, Z., & Tang, B. (2018). Surface damage mitigation of TC4 alloy via micro arc oxidation for oil and gas exploitation application: Characterizations of microstructure and evaluations on surface performance. *Applied Surface Science*, *436*, 467-476.
6. Vishnu, J., & Manivasagam, G. (2021). Surface modification and biological approaches for tackling titanium wear-induced aseptic loosening. *Journal of Bio-and Tribo-Corrosion*, *7*, 1-19.
7. Rautray, T. R., Narayanan, R., Kwon, T. Y., & Kim, K. H. (2010). Surface modification of titanium and titanium alloys by ion implantation. *Journal of Biomedical Materials Research Part B: Applied Biomaterials*, *93*(2), 581-591.
8. Garcia-Alonso, D., Serres, N., Demian, C., Costil, S., Langlade, C., & Coddet, C. (2011). Pre-/during-/post-laser processes to enhance the adhesion and mechanical properties of thermal-sprayed coatings with a reduced environmental impact. *Journal of Thermal Spray Technology*, *20*, 719-735.

9. Luo, Y., Jiang, H., Cheng, G., & Liu, H. (2011). Effect of carburization on the mechanical properties of biomedical grade titanium alloys. *Journal of Bionic Engineering*, *8*(1), 86-89.
10. Karimoto, T., & Nishimoto, A. (2019). Simultaneous boronizing and carburizing of titanium via spark plasma sintering. *Materials Transactions*, *60*(11), 2387-2391.
11. Morozow, D., Barlak, M., Werner, Z., Pisarek, M., Konarski, P., Zagórski, J., Rucki,M., Chałko, L., Łagodziński, M., Narojczyk, J., Krzysiak, Z. & Caban, J. (2021). Wear resistance improvement of cemented tungsten carbide deep-hole drills after ion implantation. *Materials*, *14*(2), 239.
12. Bhosale, D. G., Prabhu, T. R., & Rathod, W. S. (2020). Sliding and erosion wear behaviour of thermal sprayed WC-Cr3C2-Ni coatings. *Surface and Coatings Technology*, *400*, 126192.
13. Sahu, J. N., & Sasikumar, C. (2019). Development of hard and wear resistant surface coating on Ni-Cr-Mo steel by surface mechano-chemical carburization treatment (SMCT). *Journal of Materials Processing Technology*, *263*, 285-295.
14. Cheng, G., Guo, F., E, J., Zhao, G., Zhang, Z., & Jia, X. (2022). Influence of surface morphology parameters of steel on tribological properties between glass-fiber-reinforced polytetrafluoroethylene composites and steel under dry-friction and oil-lubrication conditions. *Polymer Composites*, *43*(3), 1383-1394.
15. Guo,J., Wang, F., Liou, J. J. and Liu,Y. (2022). Tribological properties of picosecond laser-textured titanium alloys under different lubrication conditions. *Ukrainian Journal of Physical Optics*, *23*(4), 243-255.
16. Zhan, X., Yi, P., Liu, Y., Xiao, P., Zhu, X., & Ma, J. (2020). Effects of single-and multi-shape laser-textured surfaces on tribological properties under dry friction. *Proceedings of the Institution of Mechanical Engineers, Part C: Journal of Mechanical Engineering Science*, *234*(7), 1382-1392.
17. Kumar, M., Ranjan, V., & Tyagi, R. (2020). Effect of shape, density, and an array of dimples on the friction and wear performance of laser textured bearing steel under dry sliding. *Journal of Materials Engineering and Performance*, *29*, 2827-2838.
18. Li, J., Liu, S., Yu, A., & Xiang, S. (2018). Effect of laser surface texture on CuSn6 bronze sliding against PTFE material under dry friction. *Tribology International*, *118*, 37-45.
19. Sun, J., Yi, P., Jia, H. Y., Yang, X. S., Shi, Y. J., Liu, Y., & Hao, M. (2022). Effects of morphology parameters of sinusoidal texture on tribological properties under dry friction. *Industrial Lubrication and Tribology*, *74*(2), 219-227.
20. Gaikwad, A., Vázquez-Martínez, J. M., Salguero, J., & Iglesias, P. (2022). Tribological properties of Ti6Al4V titanium textured surfaces created by laser: Effect of dimple density. *Lubricants*, *10*(7), 138.
21. Xue, X., Lu, L., Wang, Z., Li, Y., & Guan, Y. (2021). Improving tribological behavior of laser textured Ti-20Zr-10Nb-4Ta alloy with dimple surface. *Materials Letters*, *305*, 130876.
22. Stalder, A. F., Melchior, T., Müller, M., Sage, D., Blu, T., & Unser, M. (2010). Low-bond axisymmetric drop shape analysis for surface tension and contact angle measurements of sessile drops. *Colloids and Surfaces A: Physicochemical and Engineering Aspects*, *364*(1-3), 72-81.
23. Bormashenko, E., Bormashenko, Y., Stein, T., Whyman, G., & Bormashenko, E. (2007). Why do pigeon feathers repel water? Hydrophobicity of pennae, Cassie–Baxter wetting hypothesis and Cassie–Wenzel capillarity-induced wetting transition. *Journal of colloid and interface science*, *311*(1), 212-216.
24. Yu, A., Niu, W., Hong, X., He, Y., Wu, M., Chen, Q., & Ding, M. (2018). Influence of tribo-magnetization on wear debris trapping processes of textured dimples. *Tribology International*, *121*, 84-93.
25. Koura, M. M. (1980). The effect of surface texture on friction mechanisms. *Wear*, *63*(1), 1-12.
26. Wang, J., Xue, W., Gao, S., Li, S., & Duan, D. (2021). Effect of groove surface texture on the fretting wear of Ti–6Al–4V alloy. *Wear*, *486*, 204079.
27. Qin, L., Yang, H., Ni, Y., & Dong, G. (2022). Fabricating fluorosilane self-assembled molecular film on Babbitt alloy and its tribological performance. *Industrial Lubrication and Tribology*, *74*(4), 402-410.
28. Segu, D. Z., & Hwang, P. (2015). Friction control by multi-shape textured surface under pin-on-disc test. *Tribology International*, *91*, 111-117.
29. Guo, Z., Xie, X., Yuan, C., & Bai, X. (2019). Study on influence of micro convex textures on tribological performances of UHMWPE material under the water-lubricated conditions. *Wear*, *426*, 1327-1335.
30. Huang, J., Wei, S., Zhang, L., Shen, Z., Yang, Y., Yang, S., Lin,X., & Zhang, J. (2020). Preparation of Superhydrophobic 35CrMo Surface and Its Tribological Properties in Water Lubrication. *JOM*, *72*, 368-372.
31. Krbata, M., Eckert, M., Majerik, J., & Barenyi, I. (2020). Wear behaviour of high strength tool steel 90MnCrV8 in contact with Si_3N_4. *Metals*, *10*(6), 756.
32. Jung, Y. C., & Bhushan, B. (2006). Contact angle, adhesion and friction properties of micro-and nanopatterned polymers for superhydrophobicity. *Nanotechnology*, *17*(19), 4970.

Guojun Deng and Jialiang Guo. (2024). Tribological Properties of Textured Titanium-Alloy Surface Under Dry-Sliding and Water-Lubrication Conditions**.**
Ukrainian Journal of Physical Optics, *25*(2)**,** 02042 – 02052.
DOI: 10.3116/16091833/Ukr.J.Phys.Opt.2024.02043

Анотація*. Розроблено гнучке та ефективне рішення для поліпшення характеристик і продовження терміну служби титанового сплаву Ti6–Al4–V. Це рішення засноване на поєднанні комерційно доступної техніки створення структури на поверхні металу на*

основі наносекундного лазера та «самозбірної» модифікації методу нанесення молекулярної плівки. За допомогою лазерної обробки на поверхню титанового сплаву нанесено періодичні масиви ямок різної щільності та глибини. Морфологія поверхні, шорсткість і хімічний склад наших зразків проаналізовано за допомогою сканувальної електронної мікроскопії та конфокальної мікроскопії. Крім того, змочуваність поверхні модифікованого титанового сплаву оцінено за допомогою вимірювача контактного кута, що дало максимальний кут контакту 153,2°. Коефіцієнт тертя виміряно за допомогою трибометра, а механізм зношування проаналізовано шляхом вивчення морфології поверхні. В умовах сухого ковзання та змащування водою середній коефіцієнт тертя зменшується відповідно більш ніж на 20% та на 60% порівняно зі значенням, притаманним для початкової поверхні. Це зменшення пояснено зміною шорсткості поверхні та змочуваністю. Наш метод пропонує практичний і ефективний засіб підвищення змочуваності та поліпшення трибологічних характеристик поверхонь титанового сплаву.

***Ключові слова**: коефіцієнт тертя, лазерне текстурування, титанові сплави, сліди зношування, змочуваність.*